molecules

MDPI

Article

Two-Dimensional ABS_4 (A and B = Zr, Hf, and Ti) as Promising Anode for Li and Na-Ion Batteries

Shehzad Ahmed [1,*], Imran Muhammad [2], Awais Ghani [3], Iltaf Muhammad [1], Naeem Ullah [1], Nadeem Raza [4], Yong Wang [5], Xiaoqing Tian [1,6,*], Honglei Wu [1,*] and Danish Khan [7,*]

1 College of Physics and Optoelectronic Engineering, Shenzhen University, Shenzhen 518060, China; iltaf.muhammad@szu.edu.cn (I.M.); naeeman259@szu.edu.cn (N.U.)
2 Department of Chemistry and Guangdong Provincial, Southern University of Science and Technology, Shenzhen 518055, China; imrankhan@sustech.edu.cn
3 Smart Materials for Architecture Research Lab, Innovation Center of Yangtze River Delta, Zhejiang University, Hangzhou 314100, China; awaisghani@zju.edu.cn
4 Chemistry Department, Imam Mohammad Ibn Saud Islamic University (IMSIU), Riyadh 11623, Saudi Arabia; nadeemr890@gmail.com
5 School of Physics, Nankai University, Tianjin 300071, China; yongwang@nankai.edu.cn
6 National Laboratory of Solid-State Microstructures, Nanjing University, Nanjing 210093, China
7 College of New Materials and New Energies, Shenzhen Technology University, Shenzhen 518118, China
* Correspondence: ahmed@szu.edu.cn (S.A.); xqtian@szu.edu.cn (X.T.); hlwu@szu.edu.cn (H.W.); khandanish@sztu.edu.cn (D.K.)

Abstract: Metal ion intercalation into van der Waals gaps of layered materials is vital for large-scale electrochemical energy storage. Transition-metal sulfides, ABS_4 (where A and B represent Zr, Hf, and Ti as monolayers as anodes), are examined as lithium and sodium ion storage. Our study reveals that these monolayers offer exceptional performance for ion storage. The low diffusion barriers enable efficient lithium bonding and rapid separation while all ABS_4 phases remain semiconducting before lithiation and transition to metallic states, ensuring excellent electrical conductivity. Notably, the monolayers demonstrate impressive ion capacities: 1639, 1202, and 1119 mAh/g for Li-ions, and 1093, 801, and 671 mAh/g for Na-ions in $ZrTiS_4$, $HfTiS_4$, and $HfZrS_4$, respectively. Average voltages are 1.16 V, 0.9 V, and 0.94 V for Li-ions and 1.17 V, 1.02 V, and 0.94 V for Na-ions across these materials. Additionally, low migration energy barriers of 0.231 eV, 0.233 eV, and 0.238 eV for Li and 0.135 eV, 0.136 eV, and 0.147 eV for Na make ABS_4 monolayers highly attractive for battery applications. These findings underscore the potential of monolayer ABS_4 as a superior electrode material, combining high adsorption energy, low diffusion barriers, low voltage, high specific capacity, and outstanding electrical conductivity.

Keywords: DFT study; ternary sulfides; two-dimensional materials; electronic structure; Li and Na ion storage; binding energy; ion diffusion barriers

Citation: Ahmed, S.; Muhammad, I.; Ghani, A.; Muhammad, I.; Ullah, N.; Raza, N.; Wang, Y.; Tian, X.; Wu, H.; Khan, D. Two-Dimensional ABS_4 (A and B = Zr, Hf, and Ti) as Promising Anode for Li and Na-Ion Batteries. *Molecules* **2024**, *29*, 5208. https://doi.org/10.3390/molecules29215208

Academic Editors: Sergei Manzhos and Xiaomin Xu

Received: 10 September 2024
Revised: 30 October 2024
Accepted: 31 October 2024
Published: 4 November 2024

1. Introduction

Acquiring high energy and power densities in electrochemical storage devices is essential for developing portable electronics. The reliability of electrode materials is crucial for the performance of lithium-ion batteries (LIBs), which have become the dominant technology in energy storage [1]. Innovative materials are essential to satisfy the growing need for high energy and power density. Although graphene is a key electrode material, its theoretical capacity of 372 mAh/g restricts its capability to fulfill the increasing power density requirements [2–5]. Electrochemical energy storage systems are highly favored technologies today, with applications ranging from smart devices and electric vehicles to extensive power grids [6–8]. Consequently, advancing the renewable energy economy hinges on developing efficient, cost-effective, eco-friendly electrochemical energy storage

solutions [9–11]. Particularly, the van der Waals (vdW) gaps in layered materials are crucial for the advancement of energy storage [12–15]. These voids facilitate effective ion intercalation and diffusion, increase conductivity and capacity, and promote stable phase transitions, all of which are critical for the advancement of high-performance, long-lasting next-generation batteries [16–19]. Delve into the groundbreaking domain of multilayer nanostructures, such as transition-metal dichalcogenides (TMDs) [20,21]. Two-dimensional (2D) materials, such as molybdenum disulfide (MoS_2) and tungsten disulfide (WS_2), provide notable benefits, including a large surface area, short diffusion routes, cost efficiency, and outstanding electrical conductivity [22,23]. Doping and alloying TMDs, such as synthesizing $Mo_{1-x}W_xS_2$ alloys, enable accurate adjustment of their crystal structures and electrical characteristics, providing a viable method for improving performance in many applications [24,25]. Advanced battery technology requires electrochemically better ternary metal sulfides to enhance performance and efficiency. $NiCo_2S_4$ and $CuFeS_2$ compounds are appropriate for sodium-ion and lithium-ion batteries due to their high conductivity and attractive redox characteristics [26–28]. In contrast, $MnNi_2S_4$ and $CoMn_2S_4$ enhance energy density and cycling stability, making them suitable for hybrid systems and energy storage [29–31]. Recent tailored nanostructures, especially nanoparticle and porous designs, can improve these sulfides' electrochemical performance. Studies on $MnNi_2S_4$ emphasize sodium-ion intercalation, advancing battery material's effectiveness and durability [32]. Ternary transition metal sulfides (TTMSs) are enabling next-generation energy storage solutions that are efficient and sustainable [33,34].

Recently, Gennevieve Macam and colleagues identified a range of TTMSs, specifically ABS_4 (with A and B being Zr, Hf, and Ti) [35]. TTMSs can be synthesized using numerous processes, each offering unique advantages. Single Source Precursors (SSPs) provide exact regulation of phase and composition [36], while hydrothermal and solvothermal techniques are environmentally sustainable and economically efficient [37]. Mechanochemical synthesis facilitates scalability, while chemical vapor deposition (CVD) is optimal for producing high-quality films [38]. Colloidal synthesis guarantees uniform dispersion, while solid-state flux or salt melt techniques yield well-crystallized compounds [39].

In the present work, we employ first-principles calculations to explore the theoretical functionality of ABS_4 materials as anode materials in alkali metal ion batteries. Initially, we confirmed the stability of the pristine ABS_4 (with A and B being Zr, Hf, and Ti) monolayer by assessing its thermodynamic stabilities. We subsequently evaluated the adsorption behavior of Li/Na-ions on the ABS_4 surface by analyzing their adsorption energies, charge density differences, and Bader charges. Furthermore, the climbing-image nudged-elastic-band (CI-NEB) approach was employed to assess the diffusion energy barriers associated with various Li/Na-ions pathways on the ABS_4 monolayer. Finally, the voltage analysis and theoretical specific storage capacity were computed for Li/Na-ions on monolayer ABS_4.

2. Computational Methods

We conducted all computations using the Vienna ab initio Simulation Package (VASP) based on Density Functional Theory (DFT) and Projector Augmented Wave (PAW) methods [40,41]. The electron–ion interaction and electron–electron exchange-correlation are investigated using the Perdew–Burke–Ernzerhof (PBE) function while maintaining a fixed cutoff energy of 550 eV for the plane-wave basis [40]. Geometric optimization is achieved using a conjugate gradient algorithm for force and energy, with thresholds set at 10^{-3} eV/Å and 10^{-6} eV. Approximately $\pm$ 25 Å of a vacuum slab was introduced along the z-axis to prevent interactions between periodic images. We employ non-spin-polarized calculations, a method widely used in similar research [42–45]. The van der Waals (vdW) interaction is incorporated for ion adsorption in the structure using the semiempirical Grimme D3 method [46]. We employed a Gaussian smearing method with a broadening parameter set to a specific value (e.g., SIGMA = 0.1 eV) to ensure proper integration over the electronic states. The Monkhorst–Pack scheme is also utilized with a mesh size of (14 $\times$ 8 $\times$ 1) for unicell and (5 $\times$ 3 $\times$ 1) for 2 $\times$ 2 $\times$ 1 supercell [47]. The diffusion pathways and energy

barriers for Li/Na ions on the ABS_4 monolayer were calculated using the climbing image nudged elastic-band (CI-NEB) method [48]. Additionally, the adsorption behavior of Li and Na on the ABS_4 substrate is examined using the same mesh size ($5 \times 3 \times 1$). At the same time, the Bader method is employed to analyze charge transfer from the metal atoms to the ABS_4 atoms. To assess thermal stability, ab initio molecular dynamics (AIMD) simulations are performed within an NVT utilizing the Nose–Hoover thermostat for temperature control, maintaining a stable 300 K and 500 K for 10 ps, employing a time step of 1 fs within a $6 \times 4 \times 1$ supercell [49]. This method provides a reliable thermal environment for investigating the dynamic behavior of ABS_4.

3. Results and Discussion

In the schematic design of conventional batteries, the intercalation and deintercalation of ions between electrodes are mechanisms by which they operate, as shown in Figure 1. The movement of electrons and ions is involved in the charge and discharging processes. The 1T phase has preference over the 2H phase for ABS_4 due to its superior electrochemical properties, which include higher ion capacities, enhanced conductivity, and lower diffusion barriers [50–52]. Consequently, it is the optimal choice for high-performance anode applications [53]. Furthermore, 1T-ABS_4 enhances hydrogen evolution catalytic performance, accelerates charge/discharge cycles, facilitates efficient electron transport, and provides superior thermal stability for high-temperature and energy storage applications [54]. Similarly, as illustrated in Figure 2a, monolayer ternary transition metal sulfides (TTMSs) can form three combinations in a monoclinic structure with the chemical formula ABS_4, where A/B = Zr, Hf, or Ti. TTMSs are derived from group IVB transition metals (Ti, Zr, Hf) and chalcogen elements (S). The 1T-phase AS_2 unit cell was enlarged into a 2×1 supercell, and one transition metal atom was swapped out for an element to construct the atomic structure [55]. Using this method, the structure of ABS_4 can be adjusted to match the configuration of ABS_4, producing three distinct compounds, e.g., $HfTiS_4$, $ZrTiS_4$, and $HfZrS_4$. TTMSs are surrounded by six sulfur atoms, resulting in a triangular prismatic or octahedral coordination geometry. TMSs are classified into multiple phases, with 1T and 2H being the most prominent, based on the layering arrangement of ABS_4 layers and this coordination. In the present work, we considered 1T-phases; the measured lattice constants of 1T-phases are a = 6.100, 6.141, 6.314 Å, and b = 3.523, 3.544, 3.644 Å, for HfTiS4, ZrTiS4, and $HfZrS_4$ consistent with findings from previous studies [54].

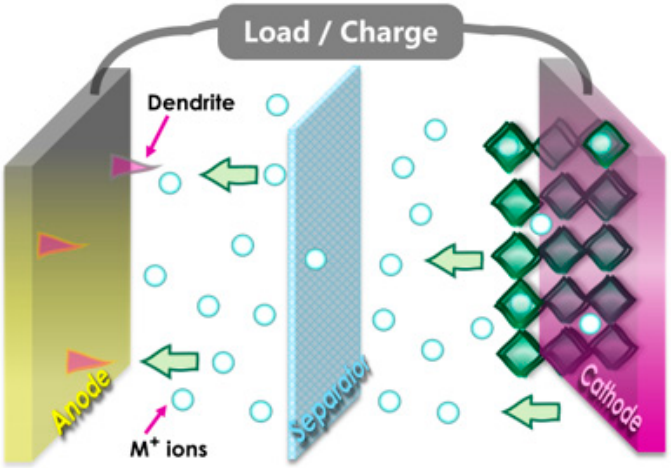

Figure 1. The Schematic illustrates the key elements, including the anode, cathode, and separator, and the flow of ions and electrons during charge and discharge cycles.

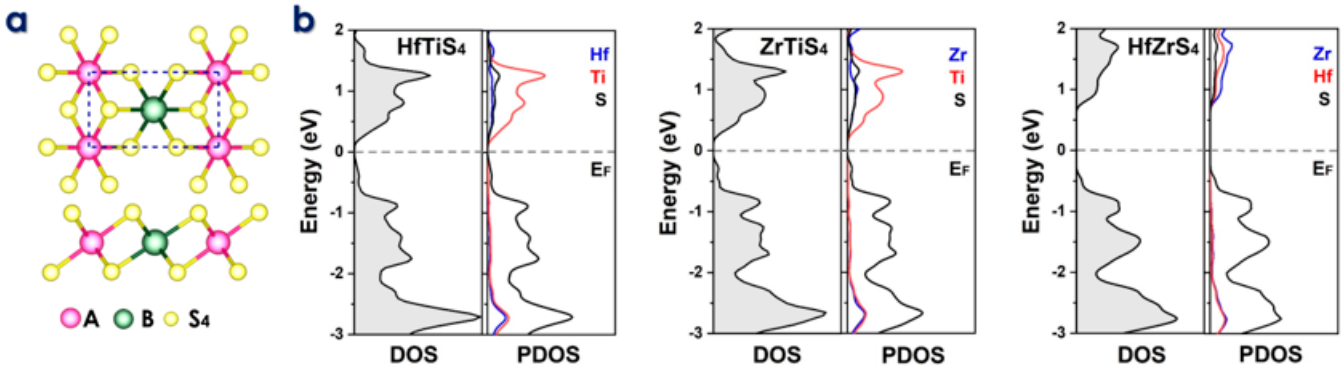

Figure 2. (**a**) Top and side views of the two-dimensional ABS_4 structure, where A and B represent Zr, Hf, and Ti. (**b**) Density of States (DOS) and Partial Density of States (PDOS) plots for $HfTiS_4$, $ZrTiS_4$, and $HfZrS_4$, illustrating their electronic properties.

The electronic characteristics of TTMSs can be better understood using Density of states (DOS) and partial density of states (PDOS) analysis. They reveal the distribution of electronic states at the Fermi level, which is essential for predicting conductivity and electrochemical performance. DOS reveals energy gaps and conducting behavior, while PDOS shows how certain atomic orbitals (e.g., metal or sulfur atoms) affect electronic states, improving understanding of ion adsorption and charge transfer. We evaluated DOS, which refers to a narrow bandgap $HfTiS_4$ (0.18 eV), $ZrTiS_4$ (0.21 eV), and $HfZrS_4$ (1.12 eV). Partial density of states (PDOS) analysis highlights the total and varying contributions of different elements (Hf, Ti, Zr, and S) to the electronic states near the Fermi level in the ABS_4. These contributions show how each element affects TTMS's electronic structure, as shown in Figure 2b. Additionally, the thermal stability of the ABS_4 monolayers was evaluated using finite temperature molecular dynamics calculations at temperatures including 300 K and 500 K, as depicted in Figure S1. The ab initio molecular dynamics simulations confirm the high stability of these structures. Performance analysis of ABS_4 as a potential anode material for Li/Na- ion batteries. The primary criterion for battery application is the adsorption strength of metal ions on a substrate. Therefore, our initial investigation uses the following equation to determine this adsorption strength.

$$E_{ads} = (E_{Mx(ABS4)} - E_{ABS4} - xE_M)/x \quad (1)$$

In the above equation, $E_{Mx(ABS4)}$ is the total energy of the ABS_4 monolayer with adsorbed Li/Na, E_{ABS4} is the intrinsic total energy of the $2 \times 2 \times 1$ ABS_4 supercell, and E_M is the energy per atom derived from the bulk material of Li/Na. According to the ABS_4 geometric symmetry, three distinct adsorption sites, a, b, and c for Li/Na-ions, labeled as follows: above the A atom (b), above the B atom (c), and the S atom (a), as shown in Figure 3a.

Indicates that Li atoms prefer to adsorb at the b-site, with an energy of 2.12, 2.09, 1.55 eV, and 2.14, 2.16, 1.51 eV for Na-ions. The computed adsorption energy E_{ads} of Li and Na on each site are given in Figure 3b. The ABS_4 monolayers have adsorption energies between these values (Figure 3b). The results indicate that the ABS_4 monolayers exhibit favorable adsorption energies. The findings suggest that ABS_4 monolayers effectively inhibit the formation of dendrites or metal clusters on the electrode surface. The charge density difference between the Li/Na ions and ABS_4 monolayers is studied with an iso-surface value of 0.004 e per $Bohr^3$, where the green and red colors show the charge gain and loss, respectively (Figure 3c). The charge transfer of Li/Na-ions is illustrated through the calculation of the charge density difference, defined as

$$\Delta\rho = \rho_{M(ABS4)} - \rho_M - \rho_{ABS4} \quad (2)$$

whereas $\rho_{M(ABS4)}$ is the charge density of the alkali metal ABS4 monolayer, ρ_M is the charge density of a Li/Na-ion, and ρ_{ABS4} is the charge density of the ABS_4 system. The findings are depicted in Figure 3c, where blue and red colors indicate charge gain and loss, respectively. These graphs show that the ABS_4 monolayers accumulate charge while the Li/Na ions lose charge, suggesting that the ionized Li/Na atoms transfer their charges to the monolayers. The electrical characteristics using Bader charge analysis to measure Li/Na-ions charge transfer to the ABS_4 monolayer. As previously found, Li/Na-ions transfer 0.86/0.84 |e|, 0.87/0.84 |e|, 0.87/0.84 |e| to site-b for $HfTiS_4$, $ZrTiS_4$, and $HfZrS_4$, as shown in Figure 3c.

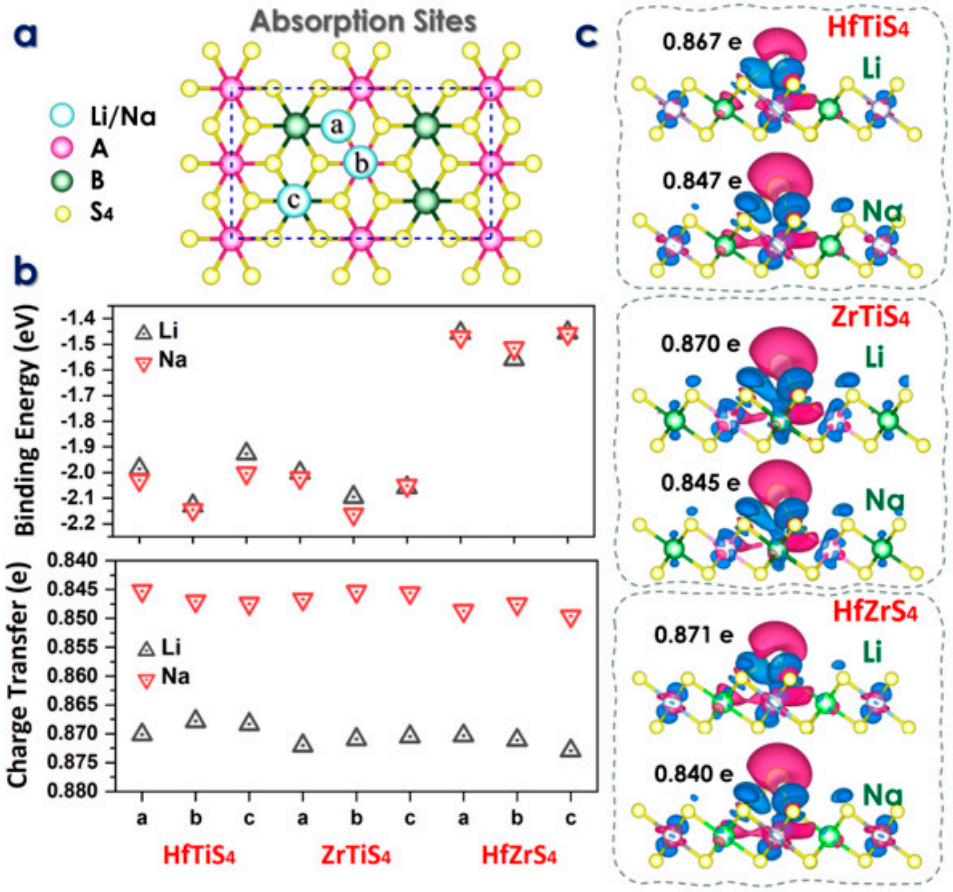

Figure 3. (**a**) Schematic illustration of three absorption sites. (**b**) Binding energy at each absorption site and charge transfer analysis (**c**) Charge density difference maps at the stable adsorption sites for Li and Na ions in $HfTiS_4$, $ZrTiS_4$, and $HfZrS_4$.

The rate of Li/Na-ions migration through the electrolyte and electrodes dramatically affects the performance of batteries. Materials with high electrical conductivity enable quick electron transfer and reduce diffusion lengths for lithium-ion migration, improving power capability. To migrate, intercalating ions must move. The climbing image nudged elastic band (CI-NEB) approach calculates diffusion barriers and minimal energy pathways (MEP) for Li/Na-ions migration on the $HfTiS_4$, $ZrTiS_4$, and $HfZrS_4$ monolayers (Figure 4a). Figure 4b shows the migration path Li-ions, the energy barriers along PATH-I were 0.231 eV, 0.233 eV, and 0.238 eV for $HfTiS_4$, $ZrTiS_4$, and $HfZrS_4$, respectively. PATH-II showed barriers of 0.251 eV, 0.260 eV, and 0.290 eV. Similarly, for Na ions, the barriers for PATH-I were 0.135 eV, 0.136 eV, and 0.147 eV; and for PATH-II, they were 0.158 eV, 0.150 eV, and 0.137 eV for $HfTiSe_4$, $ZrTiS_4$, and $HfZrS_4$, respectively. The diffusion barrier is low as compared to the largely reported anode material [55–59].

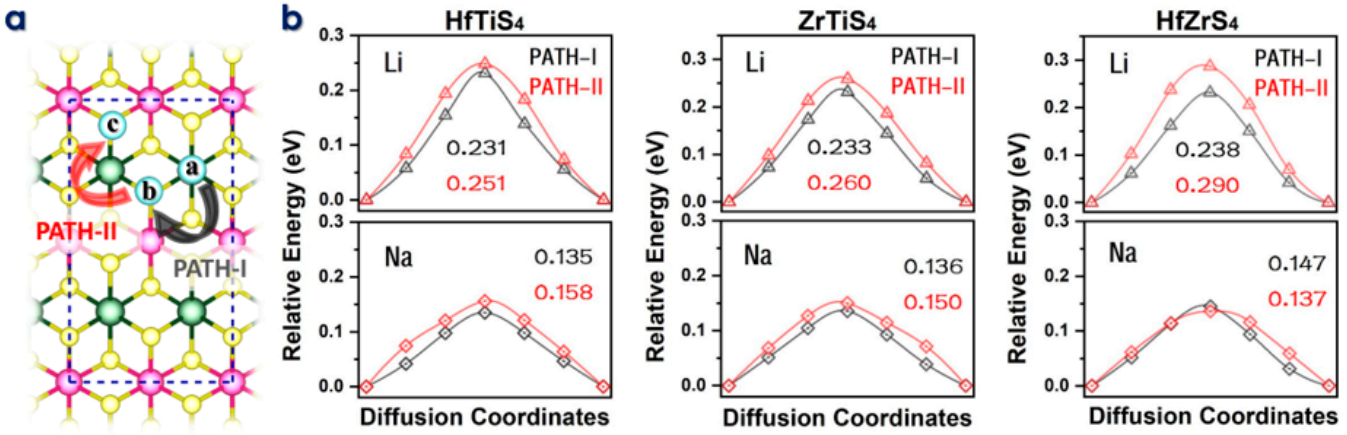

Figure 4. (**a**) Schematic illustration of two ion diffusion paths in $HfTiS_4$, $ZrTiS_4$, and $HfZrS_4$. (**b**) Diffusion barriers for Li and Na ions in $HfTiS_4$, $ZrTiS_4$, and $HfZrS_4$, including their corresponding energy barriers.

The electrochemical efficiency of batteries is the theoretical specific capacity (C) and average voltage (AV). The adsorption energies (E_{ad}) of Li and Na ions on $HfTiS_4$, $ZrTiS_4$, and $HfZrS_4$ were computed for ion concentrations ranging from 0.1 to 3.0 M_x for Li ions and from 0.1 to 2.0 M_x for Na ions (Figure 5a). We consider seven different Li/Na-ion concentrations for all structures to evaluate the maximum storage capacity; the binding energy decreases as the metal ion concentration M_x increases; the decrease in B.E is mainly due to the repulsive forces between neighboring ions. The theoretical capacity was calculated by using the following equation:

$$C = xF/3.6M_{ABS4} \quad (3)$$

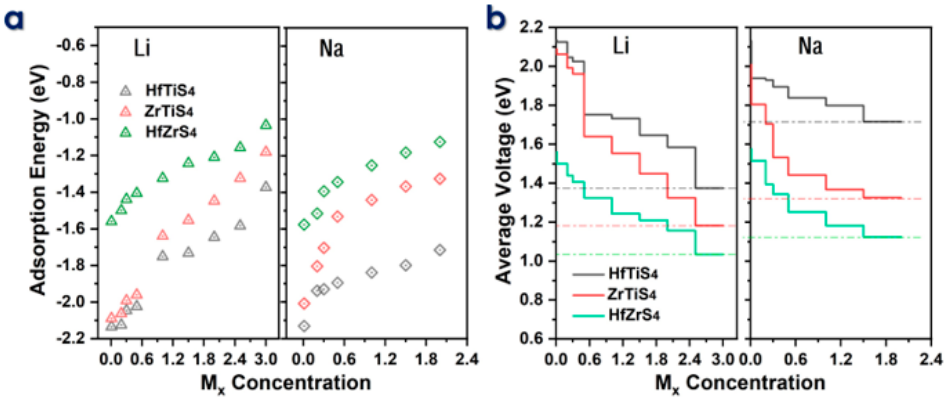

Figure 5. (**a**) Adsorption energy of $HfTiS_4$, $ZrTiS_4$, and $HfZrS_4$ as a function of metal ion concentration. (**b**) Voltage profile for Li and Na ions as a function of metal ion content, illustrating their electrochemical behavior.

In the equation, (x) represents the total number of adsorbed Li/Na ions in ABS_4, while F denotes Faraday's constant, which is 96,485.3329 s A mol^{-1}, and (M) stands for the molar mass of ABS_4, while 3.6 serves as a conversion factor related to the stoichiometry of ion intercalation. Specifically, the Li-ion capacities are 1639 mA/h, 1202 mA/h, and 1119 mA/h, and the Na-ion capacities are 1093 mA/h, 801 mA/h, and 671 mA/h for $ZrTiS_4$, $HfTiS_4$, and $HfZrS_4$, respectively. The predicted capacity is much higher than that of well-known 2D anode materials [60–63]. Theoretically, capacity concerning concentration, as shown in Figure 5b, is utilized in the following equation to calculate the average voltage for a monolayer.

$$V = -[E_{MxABS4} - E_{ABS4} - xE_{Li/Na}]/Zxe \quad (4)$$

In the above equation, E_{ABS4} and E_{MxABS4} represent the energy of the ABS_4 monolayer and the energy after Li/Na-ions adsorbed ABS_4, respectively, $E_{Li/Na}$ is the energy of the Li/Na ions in the bulk system, and (x) indicates the total number of Li/Na ions adsorbed. Li-ions average voltages of 1.16 V, 0.9 V, and 0.94 V, whereas Na-ions have 1.17 V, 1.02 V, and 0.94 V for $ZrTiS_4$, $HfTiS_4$, and $HfZrS_4$. All the average voltage values for Li and Na, as shown in Figure 5b, are within the acceptable voltage range. The calculated average voltages confirm that ABS_4 is a suitable material for the anode, contributing to the high output voltage of the batteries [43,64,65].

The DOS and PDOS are crucial for understanding the electronic behavior of monolayers like $HfTiS_4$, $ZrTiS_4$, and $HfZrS_4$ while adsorbing Li and Na ions. DOS and PDOS identify localized states near the Fermi level when a single ion is adsorbed, showing how it interacts with the host monolayer (Figure 6a). The PDOS shows hybridization between the ions orbitals (e.g., Li 2s/Na 2p) and those of the host atoms, helping explain electronic structure alterations, including band gap changes and conductivity shifts. DOS and PDOS indicate ion accumulation affects the ABS_4 electronic structure in the completely adsorbed state, frequently causing larger energy changes and conducting behavior (Figure 6b). The results indicated that all the structures retain their metallic character for fully adsorbed structures. Understanding these ABS_4 electrochemical activity, charge mobility, and ion storage capacity helps determine their viability for energy storage applications. Prospective areas of research were delineated, involving studies on alternative ion types and alterations to material characteristics for enhanced performance. Furthermore, it addresses problems associated with the experimental implementation of these materials, including scalability, stability, and the development of a solid-electrolyte interphase (SEI). Ternary metal sulfides exhibit substantial theoretical capacities and advantageous electrochemical properties; nonetheless, they encounter constraints that impede their application in battery technologies. It is essential to address stability, ion diffusion, structural integrity, and reversibility to improve the practicality and efficacy of these materials in contemporary battery systems. Additional research and development are essential to address these difficulties and enhance performance.

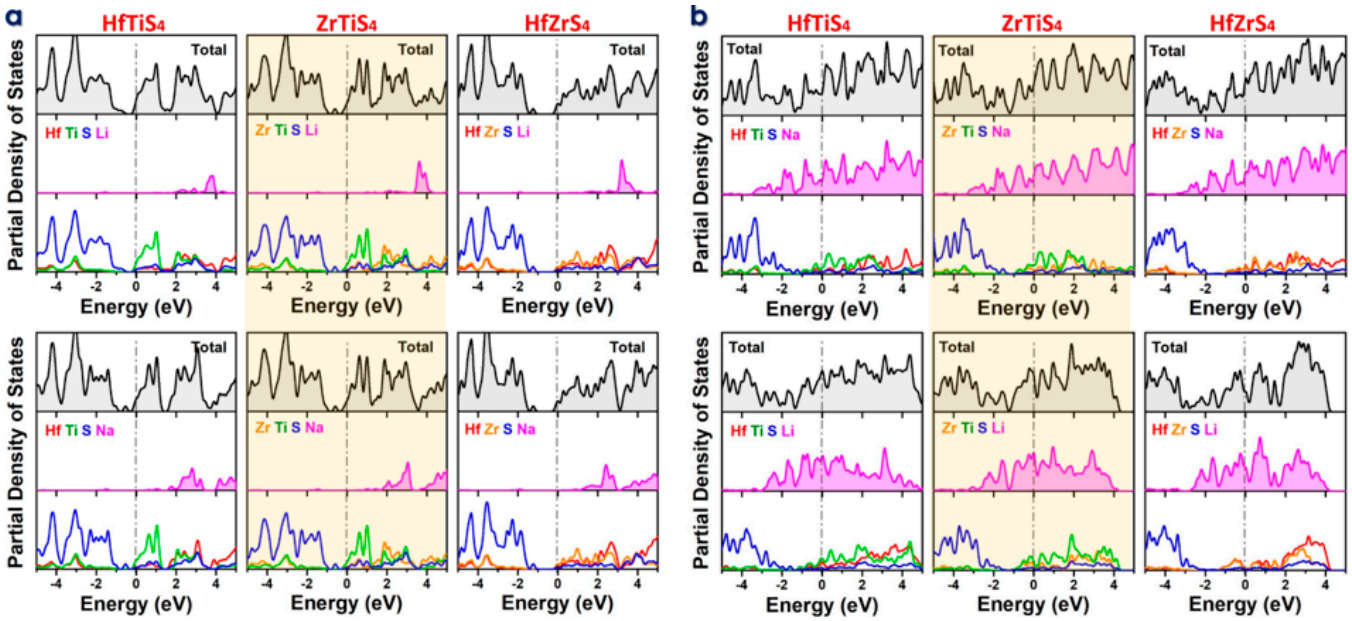

Figure 6. Density of States (DOS) and Partial Density of States (PDOS) for $HfTiS_4$, $ZrTiS_4$, and $HfZrS_4$ (**a**) Absorption of a single Li/Na-ion. (**b**) Fully adsorbed Li/Na-ions.

4. Conclusions

In conclusion, our study highlights the remarkable advancements in identifying high-performance anode materials for metal-ion batteries, focusing on ternary transition metal

sulfides (TTMSs) analyzed through density functional theory (DFT). We investigated the ABS_4 monolayer structures, where A and B are Hf, Ti, and Zr, revealing their exceptional potential as anode materials. Our first-principles analysis uncovered several critical advantages of these materials, including their metallic behavior and stability across a range of Li and Na adsorption concentrations. Notably, ABS_4 monolayers exhibit impressive performance metrics: $HfTiS_4$ stands out with the highest specific capacities of 1639 mAh/g for lithium and 1093 mAh/g for sodium. The average operating voltages are within the optimal range, at 1.16 V for lithium and 1.17 V for sodium. Furthermore, the low energy barriers of 0.231 eV for lithium and 0.251 eV for sodium facilitate efficient ion diffusion, leading to rapid charge and discharge capabilities. These findings underscore that ABS_4 monolayers are promising candidates for high-performance anodes in lithium and sodium-ion batteries, combining high specific capacity, favorable voltage profiles, and swift ion transport. Our results advocate for the potential of ABS_4 monolayers as superior materials for next-generation energy storage technologies.

Supplementary Materials: The following supporting information can be downloaded at: https://www.mdpi.com/article/10.3390/molecules29215208/s1, Figure S1 Energy evolution and structural dynamics of ZrTiS4, HfTiS4, HfZrS4.

Author Contributions: S.A.: data curation, formal analysis, calculations, writing—original draft. A.G.: validation, software. I.M. (Imran Muhammad): validation, visualization, review. I.M. (Iltaf Muhammad) and Y.W.: conceptualization, writing—review. D.K., N.U. and N.R.: funding acquisition, editing. X.T.: supervision. H.W.: funding acquisition. All authors have read and agreed to the published version of the manuscript.

Funding: This work was supported by the National Natural Science Foundation of China (Grant Number 62474113) (Grant Number 62250410369) and (Grant Number 12074195), Science and Technology Innovation Commission of Shenzhen (JCYJ20210324093007020), Shenzhen Science and Technology Program (No. 20231128110928003) and (JCYJ20190808121405740). We thank the Basic and Applied Basic Research Foundation of Guangdong Province (2021A1515010082).

Institutional Review Board Statement: Not applicable.

Informed Consent Statement: Not applicable.

Data Availability Statement: The data presented in this study are available upon request from the corresponding author.

Conflicts of Interest: The authors declare no conflicts of interest.

References

1. Tarascon, J.-M.; Armand, M. Issues and challenges facing rechargeable lithium batteries. *Nature* **2001**, *414*, 359–367. [CrossRef] [PubMed]
2. Arico, A.S.; Bruce, P.; Scrosati, B.; Tarascon, J.-M.; Van Schalkwijk, W. Nanostructured materials for advanced energy conversion and storage devices. *Nat. Mater.* **2005**, *4*, 366–377. [CrossRef]
3. Kang, B.; Ceder, G. Battery materials for ultrafast charging and discharging. *Nature* **2009**, *458*, 190–193. [CrossRef]
4. Yoo, E.; Kim, J.; Hosono, E.; Zhou, H.-S.; Kudo, T.; Honma, I. Large Reversible Li Storage of Graphene Nanosheet Families for Use in Rechargeable Lithium Ion Batteries. *Nano Lett.* **2008**, *8*, 2277–2282. [CrossRef]
5. Ahmad, M.; Chen, J.; Liu, J.; Zhang, Y.; Song, Z.; Afzal, S.; Raza, W.; Zeb, L.; Mehmood, A.; Hussain, A. Metal-organic framework-based single-atom electro-/photocatalysts: Synthesis, energy applications, and opportunities. *Carbon Energy* **2024**, *6*, e382. [CrossRef]
6. Chen, H.; Cong, T.N.; Yang, W.; Tan, C.; Li, Y.; Ding, Y. Progress in electrical energy storage system: A critical review. *Prog. Nat. Sci.* **2009**, *19*, 291–312. [CrossRef]
7. Wang, Z.; Cai, J.; Han, Y.; Han, T.; Chen, A.; Ye, S.; Liu, J.; Li, J. Computational screening of spinel structure cathodes for Li-ion battery with low expansion and rapid ion kinetics. *Comput. Mater. Sci.* **2022**, *204*, 111187. [CrossRef]
8. Idrees, M.; Batool, S.; Din, M.A.U.; Javed, M.S.; Ahmed, S.; Chen, Z. Material-structure-property integrated additive manufacturing of batteries. *Nano Energy* **2023**, *109*, 108247. [CrossRef]
9. Bertaglia, T.; Costa, C.M.; Lanceros-Méndez, S.; Crespilho, F.N. Eco-friendly, sustainable, and safe energy storage: A nature-inspired materials paradigm shift. *Mater. Adv.* **2024**, *5*, 7534–7547. [CrossRef]

10. Sharma, A.; Sharma, R.; Thakur, R.C.; Singh, L. An overview of deep eutectic solvents: Alternative for organic electrolytes, aqueous systems & ionic liquids for electrochemical energy storage. *J. Energy Chem.* **2023**, *82*, 592–626. [CrossRef]
11. Rehman, W.U.; Jiang, Z.; Qu, Z.; Ahmed, S.; Ghani, A.; Xu, Y. Highly crystalline Prussian blue cubes filled with tin oxide as anode materials for lithium-ion batteries. *Appl. Surf. Sci.* **2022**, *604*, 154533. [CrossRef]
12. Tantis, I.; Talande, S.; Tzitzios, V.; Basina, G.; Shrivastav, V.; Bakandritsos, A.; Zboril, R. Non-van der Waals 2D Materials for Electrochemical Energy Storage. *Adv. Funct. Mater.* **2023**, *33*, 2209360. [CrossRef]
13. Zhou, J.; Lu, X.; Yu, M. Structure engineering of van der Waals layered transition metal-containing compounds for aqueous energy storage. *Mater. Chem. Front.* **2021**, *5*, 2996–3020. [CrossRef]
14. Li, Y.; Yan, H.; Xu, B.; Zhen, L.; Xu, C.Y. Electrochemical intercalation in atomically thin van der Waals materials for structural phase transition and device applications. *Adv. Mater.* **2021**, *33*, 2000581. [CrossRef]
15. Saeed, M.H.; Ahmed, S.; Muhammad, I.; Murtaza, I.; Ghani, A.; Ali, A.; Abdullah, R.; Khaliq, A. Molybdenum carbide nanosheet as a high capacity anode material for monovalent alkali metal-ion batteries-Theoretical investigation. *Phys. Lett. A* **2020**, *384*, 126688. [CrossRef]
16. Cao, Y.; Li, M.; Liu, J.; Amine, K. Bridging the academic and industrial metrics for next-generation practical batteries. *Nat. Nanotechnol.* **2019**, *14*, 200–207. [CrossRef] [PubMed]
17. Wu, F.; Maier, J.; Yu, Y. Guidelines and trends for next-generation rechargeable lithium and lithium-ion batteries. *Chem. Soc. Rev.* **2020**, *49*, 1569–1614. [CrossRef] [PubMed]
18. Kim, H.; Jeong, G.; Kim, Y.-U.; Kim, J.-H.; Park, C.-M.; Sohn, H.-J. Metallic anodes for next generation secondary batteries. *Chem. Soc. Rev.* **2013**, *42*, 9011–9034. [CrossRef]
19. Tian, Y.; Zeng, G.; Rutt, A.; Shi, T.; Kim, H.; Wang, J.; Koettgen, J.; Sun, Y.; Ouyang, B.; Chen, T.; et al. Promises and Challenges of Next-Generation "Beyond Li-ion" Batteries for Electric Vehicles and Grid Decarbonization. *Chem. Rev.* **2020**, *121*, 1623–1669. [CrossRef]
20. Dumcenco, D.O.; Kobayashi, H.; Liu, Z.; Huang, Y.-S.; Suenaga, K. Visualization and quantification of transition metal atomic mixing in Mo1− x W x S2 single layers. *Nat. Commun.* **2013**, *4*, 1351. [CrossRef]
21. Song, J.-G.; Ryu, G.H.; Lee, S.J.; Sim, S.; Lee, C.W.; Choi, T.; Jung, H.; Kim, Y.; Lee, Z.; Myoung, J.-M.; et al. Controllable synthesis of molybdenum tungsten disulfide alloy for vertically composition-controlled multilayer. *Nat. Commun.* **2015**, *6*, 7817. [CrossRef] [PubMed]
22. Li, X.L.; Li, T.C.; Huang, S.; Zhang, J.; Pam, M.E.; Yang, H.Y. Controllable synthesis of two-dimensional molybdenum disulfide (MoS2) for energy-storage applications. *ChemSusChem* **2020**, *13*, 1379–1391. [CrossRef] [PubMed]
23. Li, C.; Sang, D.; Ge, S.; Zou, L.; Wang, Q. Recent Excellent Optoelectronic Applications Based on Two-Dimensional WS_2 Nanomaterials: A Review. *Molecules* **2024**, *29*, 3341. [CrossRef] [PubMed]
24. Raza, W.; Shaheen, A.; Khan, N.A.; Kim, K.H.; Cai, X. Advanced strategies for the synthesis and modulation of 2D layered heterostructures for energy conversion and storage applications. *Prog. Mater. Sci.* **2024**, *146*, 101325. [CrossRef]
25. Qin, J.; Zhao, W.; Hu, X.; Li, J.; Ndokoye, P.; Liu, B. Exploring the N2 Adsorption and Activation Mechanisms over the 2H/1T Mixed-Phase Ultrathin $Mo_{1-x}W_xS2$ Nanosheets for Boosting N2 Photosynthesis. *ACS Appl. Mater. Interfaces* **2021**, *13*, 7127–7134. [CrossRef]
26. Xue, G.; Bai, T.; Wang, W.; Wang, S.; Ye, M. Recent advances in various applications of nickel cobalt sulfide-based materials. *J. Mater. Chem. A* **2022**, *10*, 8087–8106. [CrossRef]
27. Zhang, C.; Cai, X.; Qian, Y.; Jiang, H.; Zhou, L.; Li, B.; Lai, L.; Shen, Z.; Huang, W. Electrochemically Synthesis of Nickel Cobalt Sulfide for High-Performance Flexible Asymmetric Supercapacitors. *Adv. Sci.* **2018**, *5*, 1700375. [CrossRef]
28. Chen, X.; Liu, Q.; Bai, T.; Wang, W.; He, F.; Ye, M. Nickel and cobalt sulfide-based nanostructured materials for electrochemical energy storage devices. *Chem. Eng. J.* **2021**, *409*, 127237. [CrossRef]
29. Pramanik, A.; Sengupta, S.; Saju, S.K.; Chattopadhyay, S.; Kundu, M.; Ajayan, P.M. Ternary Metal Sulfides as Electrode Materials for Na/K-Ion Batteries and Electrochemical Supercapacitor: Advances/Challenges and Prospects. *Adv. Energy Mater.* **2024**, *14*, 202401657. [CrossRef]
30. Meyer, T.E.; Jiang, K.Z.; Peng, C.C.; Sam, Q.P.; Kang, M.; Lynch, R.P.; Rowell, J.L.; Cha, J.; Robinson, R.D. Scalable Route to Colloidal NixCo3–xS4 Nanoparticles with Low Dispersity Using Amino Acids. *ACS Mater. Au* **2023**, *3*, 501–513. [CrossRef]
31. Lv, X.; Feng, L.; Lin, X.; Ni, Y. A novel 3D MnNi2O4@MnNi2S4 core-shell nano array for ultra-high capacity electrode material for supercapacitors. *J. Energy Storage* **2022**, *47*, 103579. [CrossRef]
32. Yaseen, S.; Wattoo, A.G.; Inayat, A.; Shahid, T.; Shaik, M.R.; Khan, M.; Song, Z.; Abbas, S.M. Bimetallic NiO/Mn_2O_3 nanopyramids as battery-type electrode material for high-performance supercapacitor application. *Electrochim. Acta* **2023**, *470*, 143340. [CrossRef]
33. Kulkarni, P.; Nataraj, S.K.; Balakrishna, R.G.; Nagaraju, D.H.; Reddy, M.V. Nanostructured binary and ternary metal sulfides: Synthesis methods and their application in energy conversion and storage devices. *J. Mater. Chem. A* **2017**, *5*, 22040–22094. [CrossRef]
34. Pramanik, A.; Chattopadhyay, S.; De, G.; Mahanty, S. Design of cuboidal $FeNi_2S_4$-rGO-MWCNTs composite for lithium-ion battery anode showing excellent half and full cell performances. *Batteries* **2022**, *8*, 261. [CrossRef]

35. Macam, G.; Sufyan, A.; Huang, Z.-Q.; Hsu, C.-H.; Huang, S.-M.; Lin, H.; Chuang, F.-C. Tuning topological phases and electronic properties of monolayer ternary transition metal chalcogenides (ABX4, A/B = Zr, Hf, or Ti; X = S, Se, or Te). *Appl. Phys. Lett.* **2021**, *118*, 111901. [CrossRef]
36. Roffey, A.; Hollingsworth, N.; Hogarth, G. Synthesis of ternary sulfide nanomaterials using dithiocarbamate complexes as single source precursors. *Nanoscale Adv.* **2019**, *1*, 3056–3066. [CrossRef]
37. Öztürk, O.; Gür, E. Layered Transition Metal Sulfides for Supercapacitor Applications. *ChemElectroChem* **2024**, *11*, e202300575. [CrossRef]
38. Baláž, M.; Tkáčiková, L.; Stahorský, M.; Casas-Luna, M.; Dutková, E.; Čelko, L.; Kováčová, M.; Achimovičová, M.; Baláž, P. Ternary and Quaternary Nanocrystalline Cu-Based Sulfides as Perspective Antibacterial Materials Mechanochemically Synthesized in a Scalable Fashion. *ACS Omega* **2022**, *7*, 27164–27171. [CrossRef]
39. McKeever, H.; Patil, N.N.; Palabathuni, M.; Singh, S. Functional Alkali Metal-Based Ternary Chalcogenides: Design, Properties, and Opportunities. *Chem. Mater.* **2023**, *35*, 9833–9846. [CrossRef]
40. Ahmad, S.; Din, H.U.; Nawaz, S.; Nguyen, S.-T.; Nguyen, C.Q.; Nguyen, C.V. First principles study of the adsorption of alkali metal ions (Li, Na, and K) on Janus WSSe monolayer for rechargeable metal-ion batteries. *Appl. Surf. Sci.* **2023**, *632*, 157545. [CrossRef]
41. Blöchl, P.E. Projector augmented-wave method. *Phys. Rev. B* **1994**, *50*, 17953. [CrossRef] [PubMed]
42. Muhammad, I.; Ahmed, S.; Cao, H.; Mahmood, A.; Wang, Y.-G. Three-Dimensional Silicene-Based Materials: A Universal Anode for Monovalent and Divalent Ion Batteries. *J. Phys. Chem. C* **2023**, *127*, 1198–1208. [CrossRef]
43. Lin, S.; Xu, M.; Wang, F.; Hao, J.; Li, Y. Ultrahigh energy density BeN monolayer: A nodal-line semimetal anode for Li-ion batteries. *Phys. Rev. Res.* **2024**, *6*, 013028. [CrossRef]
44. Yu, Y.; Guo, Z.; Peng, Q.; Zhou, J.; Sun, Z. Novel two-dimensional molybdenum carbides as high capacity anodes for lithium/sodium-ion batteries. *J. Mater. Chem. A* **2019**, *7*, 12145–12153. [CrossRef]
45. Butt, M.K.; Rehman, J.; Yang, Z.; Wang, S.; El-Zatahry, A.; Alofi, A.S.; Albaqami, M.D.; Alotabi, R.G.; Laref, A.; Jin, K.; et al. Storage of Na in 2D SnS for Na ion batteries: A DFT prediction. *Phys. Chem. Chem. Phys.* **2022**, *24*, 29609–29615. [CrossRef]
46. Grimme, S. Semiempirical GGA-type density functional constructed with a long-range dispersion correction. *J. Comput. Chem.* **2006**, *27*, 1787–1799. [CrossRef]
47. Aswathi, K.; Baskaran, N. First-principles study of beryllium substituted borophene as an anode material for Li/Na-ion batteries. *Comput. Condens. Matter* **2023**, *37*, e00845. [CrossRef]
48. Henkelman, G.; Uberuaga, B.P.; Jónsson, H. A climbing image nudged elastic band method for finding saddle points and minimum energy paths. *J. Chem. Phys.* **2000**, *113*, 9901–9904. [CrossRef]
49. Martyna, G.J.; Klein, M.L.; Tuckerman, M. Nosé–Hoover chains: The canonical ensemble via continuous dynamics. *J. Chem. Phys.* **1992**, *97*, 2635–2643. [CrossRef]
50. He, X.; Wang, R.; Yin, H.; Zhang, Y.; Chen, W.; Huang, S. 1T-MoS2 monolayer as a promising anode material for (Li/Na/Mg)-ion batteries. *Appl. Surf. Sci.* **2022**, *584*, 152537. [CrossRef]
51. Babar, S.; Hojaji, E.; Cai, Q.; Lekakou, C. DFT Simulations Investigating the Trapping of Sulfides by 1T-LixMoS2 and 1T-LixMoS2/Graphene Hybrid Cathodes in Li-S Batteries. *Batteries* **2024**, *10*, 124. [CrossRef]
52. Liu, Y.; Zhang, X.; Li, C.; Gao, N.; Li, H. $MoSe_2$ monolayer as a two-dimensional anode material for lithium-ion batteries: A first-principles study. *Colloids Surf. A Physicochem. Eng. Asp.* **2024**, *697*, 134455. [CrossRef]
53. Kour, P.; Deeksha; Yadav, K. Electrochemical performance of mixed-phase 1T/2H MoS2 synthesized by conventional hydrothermal v/s microwave-assisted hydrothermal method for supercapacitor applications. *J. Alloys Compd.* **2022**, *922*, 166194. [CrossRef]
54. Peng, C.; Shi, M.; Li, F.; Wang, Y.; Liu, X.; Liu, H.; Li, Z. Construction of 1T@2H MoS_2 heterostructures *in situ* from natural molybdenite with enhanced electrochemical performance for lithium-ion batteries. *RSC Adv.* **2021**, *11*, 33481–33489. [CrossRef] [PubMed]
55. Zribi, J.; Pierucci, D.; Bisti, F.; Zheng, B.; Avila, J.; Khalil, L.; Ernandes, C.; Chaste, J.; Oehler, F.; Pala, M. Unidirectional Rashba spin splitting in single layer WS2 (1−x) Se2x alloy. *Nanotechnology* **2022**, *34*, 075705.
56. Yang, Z.; Zheng, Y.; Li, W.; Zhang, J. Investigation of two-dimensional hf-based MXenes as the anode materials for Li/Na-ion batteries: A DFT study. *J. Comput. Chem.* **2019**, *40*, 1352–1359. [PubMed]
57. Bekeur, C.A.; Mapasha, R.E. Enhancement of electrochemical performance of monolayer SnS 2 for Li/Na-ion batteries through a sulphur vacancy: A DFT study. *J. Solid State Electrochem.* **2023**, *27*, 2445–2456. [CrossRef]
58. Ge, B.; Chen, B.; Li, L. Ternary transition metal chalcogenides Ti2PX2 (X = S, Se, Te) anodes for high performance metal-ion batteries: A DFT study. *Appl. Surf. Sci.* **2021**, *550*, 149177. [CrossRef]
59. Ghani, A.; Ahmed, S.; Murtaza, A.; Muhammad, I.; ur Rehman, W.; Zhou, C.; Zuo, W.L.; Yang, S. Bi–C monolayer as a promising 2D anode material for Li, Na, and K-ion batteries. *Phys. Chem. Chem. Phys.* **2023**, *25*, 4980–4986. [CrossRef]
60. Wu, J.; Wang, D.; Liu, H.; Lau, W.-M.; Liu, L.-M. An ab initio study of TiS_3: A promising electrode material for rechargeable Li and Na ion batteries. *RSC Adv.* **2015**, *5*, 21455–21463. [CrossRef]
61. Zhang, X.; Jin, L.; Dai, X.; Chen, G.; Liu, G. Two-Dimensional GaN: An Excellent Electrode Material Providing Fast Ion Diffusion and High Storage Capacity for Li-Ion and Na-Ion Batteries. *ACS Appl. Mater. Interfaces* **2018**, *10*, 38978–38984. [CrossRef] [PubMed]

62. Er, D.; Li, J.; Naguib, M.; Gogotsi, Y.; Shenoy, V.B. Ti_3C_2 MXene as a high capacity electrode material for metal (Li, Na, K, Ca) ion batteries. *ACS Appl. Mater. Interfaces* **2014**, *6*, 11173–11179. [PubMed]
63. Muhammad, I.; Ahmed, S.; Cao, H.; Yao, Z.; Khan, D.; Mahmood, A.; Hussain, T.; Xiong, X.-G.; Ahuja, R.; Wang, Y.-G. 3D porous sulfur-graphdiyne with splendid electrocatalytic and energy storage application. *Mater. Today Chem.* **2023**, *34*, 101756. [CrossRef]
64. Jing, Y.; Zhou, Z.; Cabrera, C.R.; Chen, Z. Metallic VS_2 Monolayer: A Promising 2D Anode Material for Lithium Ion Batteries. *J. Phys. Chem. C* **2013**, *117*, 25409–25413. [CrossRef]
65. Ghani, A.; Ahmed, S.; Murtaza, A.; Muhammad, I.; Zuo, W.L.; Yang, S. Three-Dimensional Porous Tetrakis Methane and Silane as a High-Capacity Anode Material for Monovalent and Divalent Metal Ion Batteries. *J. Phys. Chem. C* **2023**, *127*, 16802–16810. [CrossRef]